Double-diffusive natural convection of Casson fluids in an enclosure

M.S. Aghighi [a,*], A. Ammar [b], H. Masoumi [a]

[a] Department of Mechanical Engineering, Bu-Ali Sina University, 65175-38695 Hamedan, Iran
[b] Arts et Métiers ParisTech, 2 Boulevard du Ronceray, BP 93525, F-49035 Angers cedex 01, France

ARTICLE INFO

Keywords:
Double-diffusive convection
Non-newtonian fluid
Casson model
Yield stress
Finite element method

ABSTRACT

This study investigates the double-diffusive natural convection of the non-Newtonian Casson fluid in a square cavity based on the original viscoplastic stress model without simplification. Therefore, yield stress plays an essential role in understanding fluid behavior. The finite element approach provided a numerical solution to continuity, momentum, energy, and species governing equations. The governing parameters for this problem are Rayleigh number, *Ra*, yield number, *Y*, buoyancy ratio number, *Nr*, and Lewis number, *Le*. The influence of these parameters on heat and mass transfer, the morphology of yielded/unyielded regions, and fluid flow are thoroughly examined.

The results show that unyielded regions increase at high Rayleigh numbers, despite the increase in buoyancy force and consequently increased heat and mass transfer. On the other hand, as the buoyancy ratio drops, the flow's strength and heat and mass transmission diminish, leading to an increase in plug regions. Accordingly, the mechanisms influencing the growth of unyielded regions are complex and follow different patterns. However, the plug regions always grow with increasing *Y*. The results indicate that increasing the Lewis number (mass transfer) reduces the effect of the buoyancy ratio on flow, heat transfer, and the unyielded regions in every case. Quantitative analysis of the results indicates that, while buoyancy ratio affects heat and mass transfer almost equally, the Lewis number increases mass transfer up to three times the heat transfer. Meanwhile, changing the buoyancy ratio can increase the maximum yield stress to 400%, while changing the Lewis number has a maximum effect of 20%.

1. Introduction

Double-diffusive convection occurs as a result of thermal and solutal buoyancy effects caused by temperature and concentration gradients. Several numerical and experimental investigations have been conducted on this problem since it has wide applications in industries and science. Some of the fundamental ideas and circumstances required for the development of double-diffusive convection were outlined by Turner [1] in one of the early investigations on the subject. Afterward, the motion of a fluid confined between two long horizontal planes and heated and salted from below was studied by Huppert and Moore [2]. They combined perturbation analysis with a direct numerical solution of the governing equations. Linden and Shirtcliffe [3] provided a model of the diffusive interface in double-diffusive convection with a high Rayleigh number. Griffiths' research [4] revealed that layered double-diffusive convection of a fluid within a porous material is a real possibility in some cases. Costa and Weisst [5] have used a simplified model of two-dimensional thermosolutal convection to study the transition between oscillatory and steady convection. Knobloch and Proctor [6] analyzed oscillation stability in a two-dimensional nonlinear double-diffusive system. A comprehensive overview of the basic concepts and first analyses (numerical and laboratory) in this field was provided by Huppert and Turner [7].

The analysis of double-diffusive convection within an enclosure has been the subject of significant research since the early 1990s. These studies have considered different modes of buoyancy ratios and Lewis numbers. Han and Kuehn [8,9] studied the effects of horizontally imposed temperature and concentration gradients in a vertical rectangular cavity. Then, Beghein et al. [10] analyzed steady-state thermosolutal convection in a square cavity. Mamou et al. [11] considered an analytical and numerical natural convection model in a rectangular cavity containing a double-diffusive fluid with uniform heat and mass flux along the vertical sides. Xin et al. [12] explored the onset of convection in double diffusion when thermal and fluid buoyancy forces are equal and opposite. Ghorayeb and Mojtabi [13] did a similar study in a vertical rectangular cavity. The natural convection of two gasses in a trapezoidal enclosure with an induced unstable thermal stratification

* Corresponding author.
E-mail address: ms.aghighi@basu.ac.ir (M.S. Aghighi).

Nomenclature

a, b	Correlation coefficients,dimensionless
Bn	Bingham number,Eq. (13)
C	concentration, dimensionless
C_p	specific heat capacity, $kJkg^{-1}K^{-1}$
D	mass diffusivity m^2s^{-1}
g	acceleration due to gravity, ms^{-2}
H	reference value of length, m
L	length of the cavity, m
Le	Lewis number, Eq. (10)
m	Papanastasiou regularization parameter
Nr	Buoyancy ratio number, Eq. (9)
Nu	local Nusselt number,Eq. (16)
$\overline{Nu}$	average Nusselt number, Eq. (17)
p	pressure,dimensionless
p_0	reference value of pressure,Pa
Pr	Prandtl number, Eq. (7)
Ra	Rayleigh number, Eq. (8)
Sh	local Sherwood number, Eq. (16)
$\overline{Sh}$	Average Sherwood number, Eq. (17)
T	temperature of fluid, K
u	velocity component in x direction, dimensionless
u_0	reference velocity, ms^{-1}
v	velocity component in y direction, dimensionless
x, y	Cartesian coordinates,dimensionless
Y	yield number , Eq. (14)
Y_c	critical yield number,dimensionless

Greek symbols

α	thermal diffusivity of fluid, m^2s^{-1}
β_T	coefficient of thermal expansion, K^{-1}
β_C	coefficient of concentration expansion, m^3kg^{-1}
$\dot{\gamma}$	rate of strain tensor, dimensionless
θ	temperature, dimensionless
ν	kinematic viscosity, m^2s^{-1}
μ	palstic viscosity, Pas
ρ	density of fluid, kgm^{-3}
τ	stress tensor, dimensionless
τ_y	yield stress of fluid, dimensionless

Subscripts

C	cold
H	hot
r	reference value

Superscript

-	dimensional variable

has been explored numerically and experimentally by Biezen and Bruining [14]. Some scholars were also conducting comparative studies on porous medium simultaneously. Mamou et al. [15] investigated double-diffusive natural convection in a rectangular fluid-saturated vertical porous enclosure. Karimfard et al. [16] analyzed double-diffusive natural convection in a square cavity filled with a porous medium. Several flow models were considered, including Darcy flow, Forchheimer and Brinkman extensions, and generalized flow. A similar study in a rectangular enclosure was done by Nithiarasu et al. [17]. Then, Bennacer and colleagues [18] ran a numerical simulation to understand how saturated anisotropic porous media influences double-diffusive convection in a rectangular cavity.

Over the last decade, more in-depth studies have been conducted on the double diffusion process within enclosures. Given the relevance and growth of nanoscience, researchers have investigated the study of double-diffusive convection in nanofluids. Although nanofluids are typically studied for their heat transfer properties, they are a subset of heat and mass transfer problems. As a result, researchers were interested in the phenomena of double-diffusive convection in fluids with nanoparticles [19–26]. Another favorite research topic has been studying magnetic fields' effect on double-diffusive convection. Sunil et al. [27] and Teamah et al. [28,29] conducted some preliminary studies in this field, which other researchers later pursued with a focus on details [30–34]. A further investigation that caught the researcher's curiosity was the study of entropy generation in double diffusion natural convection systems [35–37]. In most of the works listed, concentration and temperature interactions (Soret and Dufour effects) have been neglected. However, some have attempted to study these effects, especially when considering natural convection [38–43].

Along with the above-stated topics, double-diffusive convection in non-Newtonian fluids has lately gained interest. Although the combined effects of nonlinear stress relationship with heat and mass transfer increase the complexity of double-diffusive convection analysis, due to the wide application of non-Newtonian fluids, achieving the results has been considered by researchers [44–49]. However, there has been no study on the double-diffusive natural convection of Casson fluid in a cavity, despite being one of the most extensively utilized and essential non-Newtonian fluids.

Casson fluids are a class of non-Newtonian fluids defined by their yield stress. When a yield (viscoplastic) material is not adequately stressed (when the stress is less than the yield stress), the material acts like a solid and does not flow. Above the yield stress, it will flow as a viscous fluid. Viscoplastic fluids are identified by three main models: Bingham [50], Herschel-Bulkley [51], and Casson [52]. The Bingham model is the simplest way to describe the behavior of viscoplastic materials. On the other hand, the Casson model is the most complicated viscoplastic model. For this reason, most of the research on heat transfer of viscoplastic materials inside the cavity is based on the Bingham model [53–58]. However, some research has been done based on Herschel-Bulkley [59,60] and Casson model [61,62].

In recent years, studies on the Double diffusive natural convection of Casson fluids have attracted considerable attention because of their essential applications such as blood, jams, paints, sewage and petroleum production, etc. [63,64]. As far as we know, no research on double-diffusive convection in an enclosure has been conducted using the Casson yield stress model. Notwithstanding, there has been a great deal of interest in this issue in many geometries. Some examples of these studies are listed below. Mohan and Satheesh analyzed the double-diffusion convection flow of Casson fluid in a lid-driven porous cavity [65]. Ahmed and co-workers [66] studied the entropy generation of double-diffusive convection of Casson fluid over a nonlinear stretching sheet. Effects of MHD and thermal radiation on the three-dimensional convective double diffusion of Casson nanofluid over a Stretching Surface have been examined by Gireesh et al. [67]. Recently, Das and co-workers [68] analyzed the effects of porosity and magnetic field on the unsteady double-diffusive Casson fluid flow past a flat plate. Moreover, Oyelakin and co-workers [69] studied the effects of convective double diffusion on the flow of a Casson nanofluid at a stagnation point. More studies on the current topic can be found in [70–74].

The purpose of this study is to explain the mechanism of double-diffusion natural convection of Casson fluids in enclosures comprehensively and in detail based on the original model without simplification. Thereby thorough analysis of the yield and unyielded regions' behaviors become achievable. Based on the literature review above, this problem has not yet been investigated, despite its wide range of applications. This study has been accomplished by developing a numerical model based on the finite element method to obtain solutions for the governing equations. The authors propose the correlations for Nusselt and Sherwood numbers, which will allow the quantification of convective exchanges in this fluid type.

2. Mathematical formulation

We consider a two-dimensional square enclosure filled with non-Newtonian Casson fluid (Fig. 1). The horizontal boundaries of the cavity are adiabatic and impermeable. Thereby, there will be no heat or concentration flux. Different concentrations and temperatures are maintained on the vertical walls. A high concentration $(\overline{C}_H)$ and temperature (T_H) are applied to the left wall, while a low concentration $(\overline{C}_C)$ and temperature (T_C) are applied to the right wall. No-slip conditions are considered at walls. We assume that the thermophysical properties of the fluid will not vary except for density in the body force, analyzed using the Boussinesq model for both temperature and concentration. Using conservation of mass, momentum, energy, and concentration in two dimensions, the following equations govern natural convection flow:

$$\begin{gathered}
\frac{\partial \overline{u}}{\partial \overline{x}} + \frac{\partial \overline{v}}{\partial \overline{y}} = 0 \\
\rho\left(\overline{u}\frac{\partial \overline{u}}{\partial \overline{x}} + \overline{v}\frac{\partial \overline{u}}{\partial \overline{y}}\right) = -\frac{\partial \overline{p}}{\partial \overline{x}} + \left(\frac{\partial \overline{\tau}_{xx}}{\partial x} + \frac{\partial \overline{\tau}_{yx}}{\partial y}\right) \\
\rho\left(\overline{u}\frac{\partial \overline{v}}{\partial \overline{x}} + \overline{v}\frac{\partial \overline{v}}{\partial \overline{y}}\right) = -\frac{\partial \overline{p}}{\partial \overline{y}} + \left(\frac{\partial \overline{\tau}_{yy}}{\partial y} + \frac{\partial \overline{\tau}_{xy}}{\partial x}\right) - \rho g \beta_T (T - T_r) - \rho g \beta_C (\overline{C} - \overline{C}_r) \\
\overline{u}\frac{\partial T}{\partial \overline{x}} + \overline{v}\frac{\partial T}{\partial \overline{y}} = \alpha\left(\frac{\partial^2 T}{\partial \overline{x}^2} + \frac{\partial^2 T}{\partial \overline{y}^2}\right) \\
\overline{u}\frac{\partial \overline{C}}{\partial \overline{x}} + \overline{v}\frac{\partial \overline{C}}{\partial \overline{y}} = \mathrm{D}\left(\frac{\partial^2 \overline{C}}{\partial \overline{x}^2} + \frac{\partial^2 \overline{C}}{\partial \overline{y}^2}\right)
\end{gathered} \tag{1}$$

According to the above definitions, the various dimensional quantities are: $\overline{u}$, horizontal velocity, $\overline{v}$, vertical velocity, T, temperature, $\overline{C}$, concentration, and $\overline{p}$, pressure.T_r and $\overline{C}_r$ are reference values of temperature and concentration ($T_r = (T_H + T_C)/2$ and $\overline{C}_r = (C_H + C_C)/2$). ρ is the density, g is the gravity acceleration, β_T and β_C are the thermal and concentration expansions, respectively. α is the thermal diffusivity, and D is the mass diffusivity.

Casson's model predicts the stress-deformation behavior as follows:

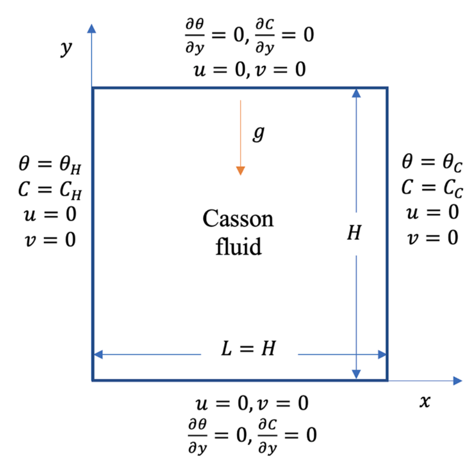

Fig. 1. Schematic diagram of the physical model and coordinate system. The horizontal boundaries of the cavity are adiabatic and impermeable. A high concentration and temperature is applied to the left wall, while a low concentration and temperature is applied to the right wall. No-slip conditions are considered at walls.

$$\begin{gathered}
\overline{\tau}_{ij} = \left(\sqrt{\mu} + \left(\frac{\tau_y}{|\bar{\dot{\gamma}}|}\right)^{\frac{1}{2}}\right)^2 \bar{\dot{\gamma}}_{ij} \ if\, |\overline{\tau}| > \tau_y \\
\bar{\dot{\gamma}} = 0 \ if\ |\overline{\tau}| < \tau_y
\end{gathered} \tag{2}$$

Here, $\overline{\tau}$ is the shear stress, $\bar{\dot{\gamma}}$ is the shear rate, μ is the plastic viscosity, τ_y is the yield stress, and $|\bar{\dot{\gamma}}|$ is the magnitude of the symmetric rate-of-strain tensor.

The dimensionless variables are obtained using the characteristic scales H for length, $u_0 = (g\beta H\Delta T)^{1/2}$ for the velocity and $p_0 = (\rho u_0^2)$ for the pressure.

The dimensionless temperature θ and concentration C are defined by:

$$\begin{gathered}
\theta = \frac{T - T_r}{T_H - T_C} \\
C = \frac{\overline{C} - \overline{C}_r}{C_H - C_C}
\end{gathered} \tag{3}$$

Based on the above assumptions, the governing equations in their nondimensionalized form can be written as:

$$\begin{aligned}
&\frac{\partial u}{\partial x} + \frac{\partial v}{\partial y} = 0 \\
&u\frac{\partial u}{\partial x} + v\frac{\partial u}{\partial y} = -\frac{\partial p}{\partial x} + Pr^{\frac{1}{2}} Ra^{\frac{-1}{2}}\left(\frac{\partial \tau_{xx}}{\partial x} + \frac{\partial \tau_{yx}}{\partial y}\right) \\
&u\frac{\partial v}{\partial x} + v\frac{\partial v}{\partial y} = -\frac{\partial p}{\partial y} + Pr^{\frac{1}{2}} Ra^{\frac{-1}{2}}\left(\frac{\partial \tau_{yy}}{\partial y} + \frac{\partial \tau_{xy}}{\partial x}\right) + (\theta + Nr.C) \\
&u\frac{\partial \theta}{\partial x} + v\frac{\partial \theta}{\partial y} = (Ra.Pr)^{\frac{-1}{2}}\left(\frac{\partial^2 \theta}{\partial x^2} + \frac{\partial^2 \theta}{\partial y^2}\right) \\
&u\frac{\partial C}{\partial x} + v\frac{\partial C}{\partial y} = \frac{1}{Le}(Ra.Pr)^{\frac{-1}{2}}\left(\frac{\partial^2 C}{\partial x^2} + \frac{\partial^2 C}{\partial y^2}\right)
\end{aligned} \tag{4}$$

Here$u$, v, θ, C, and p are non-dimensional forms of $\overline{u}, \overline{v}$, T, $\overline{C}$ and $\overline{p}$, respectively.

The relevant boundary conditions of temperature and concentration are given as follows:

$$\begin{aligned}
&\frac{\partial \theta}{\partial y} = 0\ , \frac{\partial C}{\partial y} = 0 \quad at \quad y = 0 \ and\ y = 1 \\
&\theta = 0.5, \quad C = 0.5 \quad at \quad x = 0 \\
&\theta = -0.5, \quad C = -0.5 \quad at \quad x = 1
\end{aligned} \tag{5}$$

No-slip conditions apply to the solid boundaries:

$$u = 0\ , v = 0 \quad on\ all\ walls \tag{6}$$

The non-dimensional parameters are defined as:
Prandtl number:

$$Pr = \frac{\mu C_p}{k} \tag{7}$$

Rayleigh number:

$$Ra = \frac{g\beta_T \Delta T H^3}{\alpha\nu} \tag{8}$$

Buoyancy ratio number:

$$Nr = \frac{\beta_C \Delta \mathrm{C}}{\beta_T \Delta T} \tag{9}$$

Lewis number:

$$Le = \frac{\alpha}{D} \tag{10}$$

The stress-deformation behavior of the Casson model in non-dimensional form can be written as:

$$\tau_{ij} = \left(1 + \left(\frac{Bn}{|\dot{\gamma}|}\right)^{\frac{1}{2}}\right)^{2} \dot{\gamma}_{ij} \quad if \quad |\tau| > Bn$$
$$\dot{\gamma} = 0 \quad if \quad |\tau| < Bn \tag{11}$$

In this equation, $|\tau|$ is the second invariant of the shear stress and $|\dot{\gamma}|$ is the rate-of-strain tensors. Here $\dot{\gamma}_{ij}$ is defined as below:

$$\dot{\gamma}_{ij} = \frac{\partial u_i}{\partial x_j} + \frac{\partial u_j}{\partial x_i} \tag{12}$$

The second invariant of the strain and stress tensors are:

$$|\dot{\gamma}| = \sqrt{\frac{1}{2}\dot{\gamma}_{ij}\dot{\gamma}_{ij}} \text{ and } |\tau| = \sqrt{\frac{1}{2}\tau_{ij}\tau_{ij}} .$$

Where Bn is the Bingham number:

$$Bn = (Pr/Ra)^{-1/2} \frac{\tau_y}{\rho\beta g \Delta T H} = (Pr/Ra)^{-1/2}\ Y \tag{13}$$

Here Y is the yield number:

$$Y = \frac{\tau_y}{\rho\beta g \Delta T H} \tag{14}$$

The Papanastasiou [75] regularization prevents discontinuity between yielding and unyielding regions. Hence, Eq. (11) can be rewritten as follows:

$$\tau_{ij} = \left(1 + \left(\frac{Bn}{|\dot{\gamma}|}\right)^{\frac{1}{2}} \left(1 - \exp\left(-\sqrt{m|\dot{\gamma}|}\right)\right)\right)^{2} \dot{\gamma}_{ij} \tag{15}$$

Regularization parameter m is usually set to be very large; here, it is set to $m = 10^4$. This value of m coincides with that of the non-regularized Casson model for viscosity values.

Moreover, the local Nusselt and Sherwood numbers can be written as:

$$Nu = -\left[\frac{\partial \theta}{\partial x}\right]_{x=0}$$
$$Sh = -\left[\frac{\partial C}{\partial x}\right]_{x=0} \tag{16}$$

and the mean Nusselt, $\overline{Nu}$ and Sherwood, $\overline{Sh}$ numbers are defined as follows:

$$\overline{Nu} = -\int_0^1 \left[\frac{\partial \theta}{\partial x}\right]_{x=0} dy$$
$$\overline{Sh} = -\int_0^1 \left[\frac{\partial C}{\partial x}\right]_{x=0} dy \tag{17}$$

3. Numerical methodology

Researchers have used various numerical methods to analyze heat and mass transfer problems. Utilizing a similarity solution, for example, is an optimal and practical way of analyzing flow over a plate [67,76,77] or at the stagnation point [69,78]. Still, when it comes to natural convection in the enclosure, methods based on finite elements make up one of the most common choices [79–81]. Accuracy, flexibility, and modeling are just a few benefits of using the finite element approach to solve complicated issues.

In this research, the coupled conservation equations in their non-dimensional forms (Eq. (4)) are numerically solved using the Galerkin weighted residual method of the finite element formulation. The uniform structured grid is constructed by means of nine node bi-quadratic elements. The numerical algorithm described in [61] was used to solve the discretized equations. Here, this method is developed for heat and mass transfer cases by adding the concentration equation and considering its effects on momentum equations. Therefore, the following can be stated briefly as the solution procedure:

1) The initial values of velocity variables should be considered. (These values can be assumed zero or obtained by solving Stokes linear equations.)
2) According to the known velocity values, the shear rate and stress tensor are obtained based on Eq. (12) and Eq. (15), respectively.
3) The known velocity values are also used to linearize the convective terms in the momentum, energy, and concentration equations.
4) The governing equations (4) are linearized by applying steps 2 and 3 and then discrete and integrated using the Galerkin weighted residual method of the finite element formulation (Details are provided in reference [61])
5) After applying the boundary conditions, the resulting matrix is solved using algebraic relations.
6) As new velocity values are obtained, the computational process is repeated from step 2 until convergence is achieved.

When the difference between the new and old value of velocity components, temperature, and concentration fields was less than 10^{-4}, convergence was considered to have occurred.

A grid-independent solution was ensured through a comprehensive mesh testing procedure. The deviation values in Table 1 indicate that a uniform grid of 40×40 nine node bi-quadratic elements is sufficient to achieve grid independence. Extensive comparisons between the present numerical method and the prior studies for pure Casson fluid are reported in recent studies [61,62]. Additionally, the results obtained for double-diffusion natural convection of a Newtonian fluid within a cavity with differentially heated side walls were compared with the numerical results obtained by Beghein et al. [10], Teamah et al. [29], and Oueslati et al. [36] (Fig. 2). Excellent agreement has been observed for all the results.

4. Results and discussion

Extensive new results embracing wide ranges of dimensionless parameters as yield number (fromzerotothemaximumvalue: $0 \le Y \le Y_{max}$), Rayleigh number (for the effective range of laminar flow: $10^3 \le Ra \le 10^6$), buoyancy ratio number (for cooperative buoyancy convection, $Nr = 1$, thermal buoyancy convection, $Nr = 0$, and opposing solutal buoyancy force, $Nr = -0.5$), and Lewis number (for three different ratios of thermal diffusivity to mass diffusivity: $Le < 1$, $Le = 1$, and $Le > 1$)at constant Prandtl number ($Pr = 100$ since results are not sensitive to Pr in the tested range $10 \le Pr \le 10^3$). These parameters were studied primarily for their effects on fluid flow and the thermal and concentration fields.

4.1. Effects of Rayleigh number, yield number, and buoyancy ratio

First, we consider the combined effects of Rayleigh number, yield number, and buoyancy ratio on fluid flow and solutal and thermal distributions in the enclosure. The constant value for Lewis number ($Le=1$) is considered in this section.

Fig. 3 depicts the variation of velocity profile, v, and non-dimensional temperature, θ, with Rayleigh number, Ra, at horizontal mid-plane ($y = 0.5$) of the enclosure for $Ra = 10^4, 10^5, 10^6$.

Stream functions, isotherms, and shear rate contours are also shown

Table 1
Grid independence study at $Ra = 10^5$, $Nr = 1$, $Le = 5$.

Grid	elements	nodes	$\overline{Nu}_b$	$\overline{Sh}_b$	v_{max}
G1	30×30	3721	5.086	9.936	76.96
G2	40×40	6561	5.097	10.024	76.93
G3	50×50	10, 201	5.101	10.061	76.94

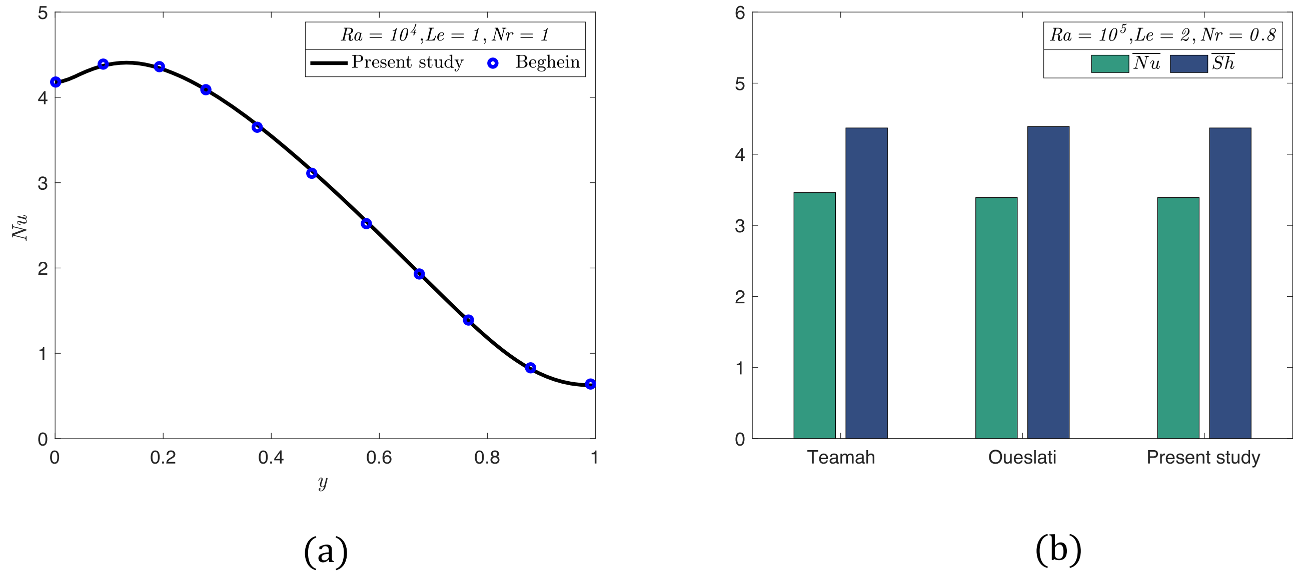

Fig. 2. Validation of the present code results for: (a) local Nusselt number $\boldsymbol{Nu}$ (present study and Beghein study [10]). (b) mean Nusselt number $\overline{\boldsymbol{Nu}}$ and mean Sherwood number $\overline{\boldsymbol{Sh}}$ (Teamah study [29], Oueslati study [36] and present study).

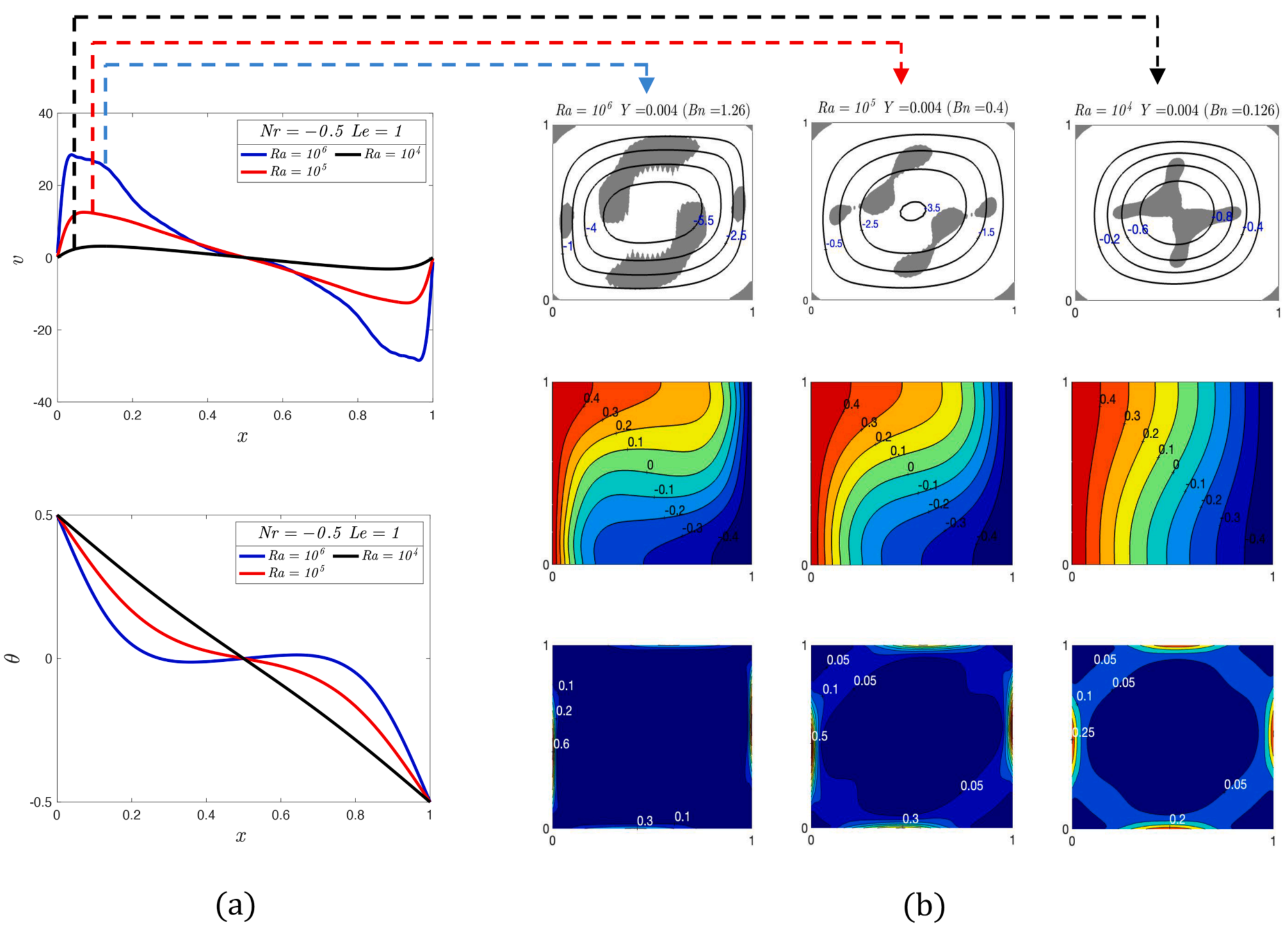

Fig. 3. Effects of Rayleigh number: (a) Variations of non-dimensional velocity (top) and non-dimensional temperature (bottom) along the horizontal mid-plane. (b) Contours of non-dimensional stream functions (top), temperature (midle), and shear rate (bottom), at $\boldsymbol{Ra} = 10^4 - 10^6$, $Y = 0.004$, Nr=−0.5,and Le=1. (Since Le=1, the temperature contours also represent the concentration contours.).

in this figure. One can see that, as Ra increases, fluid velocity increases, and the boundary layers are more closely confined to the walls due to stronger circulation. This phenomenon also increases the nonlinearity of the temperature distribution. As a result, with increasing Ra, stream functions exhibit stronger flow patterns in the cavity, and the temperature contours become more curved. Shaded parts have represented the unyielded (plug) regions in these figures. It is worth mentioning that the unyielded areas also increase with the increasing Rayleigh number. High Rayleigh numbers limit the flow circulation to thin boundary layers along the vertical walls, and hence in the center of the cavity, a large portion of the fluid is stagnant, which leads to a lower shear rate (see shear rate contours). As a result, the unyielded regions grow in this area.

Fig. 4 depicts the influence of the buoyancy ratio numbers (*Nr*) on flow properties. As can be observed, the fluid velocity is substantially larger for $Nr = 1$ than for $Nr = 0$ and -0.5, indicating cooperative buoyancy convection (both solutal buoyancy and thermal buoyancy are in the same direction). For $Nr = 0$, thermal buoyancy is the only force that drives the flow (the solutal buoyancy force does not affect the flow). As the buoyancy ratio number becomes negative ($Nr = -0.5$), the opposing solutal buoyancy force weakens the flow driven by the thermal buoyancy force. It can also be seen that, as *Nr* increases, the extent of non-linearity of temperature distribution increases, and the boundary layer is more closely confined to the walls due to stronger convection effects. Velocity vector profiles and the unyielded regions are also shown in Fig. 4 for different buoyancy ratio numbers. It is seen that decreasing the buoyancy ratio number leads to a monotonic decrease in the flow strength and causes a more uniform flow distribution inside the cavity due to weaker convective transport. As a result, unyielded areas grow with decreasing *Nr*.

On the other hand, as shown in Fig. 5, by increasing the yield number, the fluid velocity decreases inside the enclosure due to stronger viscous resistance, which suppresses the convective currents. For this reason, the temperature distribution becomes more uniform with increasing yield numbers. Velocity vector profiles show a strong (wall-inclined) flow in the Newtonian case ($Y = 0$) without unyielded areas. However, as the yield number increases, the flow's intensity decreases, its distribution becomes more uniform, and the unyielded areas subsequently increase.

Fig. 6 depicts the effects of yield number on the mean Nusselt number for the hot wall at different Rayleigh and buoyancy ratio numbers. As mentioned before, the increase in Rayleigh number strengthens the intensity of convection and improves heat and mass transfer performance. The maximum heat and mass transfer is observed for Newtonian fluid ($Y = 0$) and then decreases as Y gradually increases from $Y = 0$to the maximum yield number where dominant conductive heat and mass transfer occur. It should be mentioned here that the concentration distribution is similar to the temperature distribution because of the Lewis number (*Le=1*). Hence, the value of Sherwood and Nusselt numbers are also identical in this section.

4.1.1. Correlation for the mean Nusselt (Sherwood)number

In this section, correlations for the average Nusselt (Sherwood) number are proposed, including the Nusselt and Rayleigh numbers as well as the yield and buoyancy ratio numbers.

Using the physics of the problem, we can determine that the quantity of heat transfer at zero yield stress corresponds to Newtonian fluid, and that at maximum yield stress, it corresponds to thermal conductivity. Hence, a correlation for the mean Nusselt number of yield stress Casson fluid, $\overline{Nu}$ can be proposed in a general form as below:

$$\overline{Nu} = 1 + \left(\overline{Nu}_N - 1\right)\left[1 - \left(\frac{Y}{Y_{max}}\right)^a\right]^b \tag{18}$$

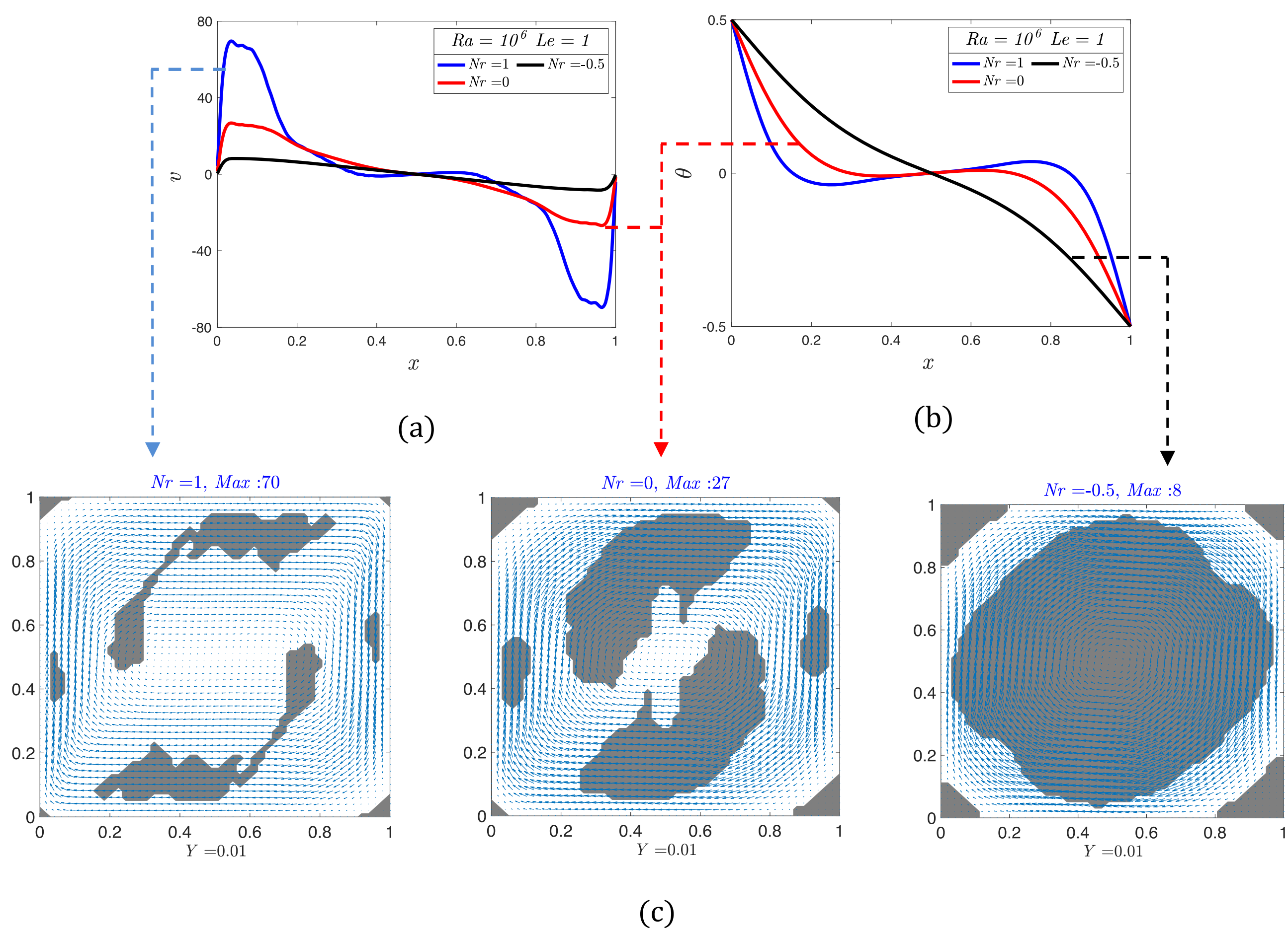

Fig. 4. Effects of buoyancy ratio number: (a) Variations of non-dimensional velocity along the horizontal mid-plane. (b) Variations of non-dimensional temperature along the horizontal mid-plane. (c) Velocity vectors and plug regions for cooperative buoyancy convection (left), thermal buoyancy convection (midle), and opposing solutal buoyancy force (right) at $\boldsymbol{Ra} = 10^6$, $\boldsymbol{Y} = 0.01$, and $\boldsymbol{Le} = 1$.

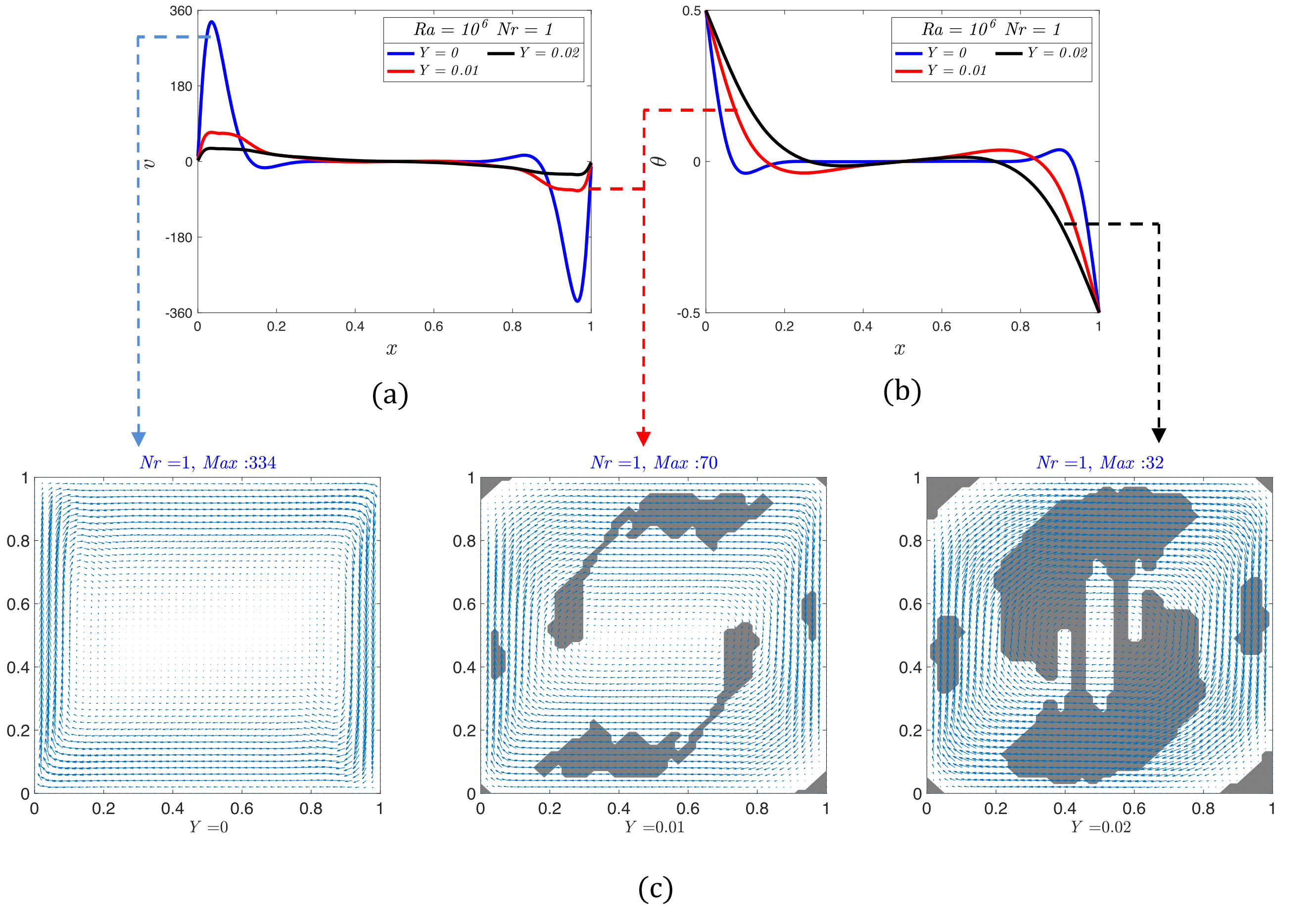

Fig. 5. Effects of yield number: (a) Variations of non-dimensional velocity along the horizontal mid-plane. (b) Variations of non-dimensional temperature along the horizontal mid-plane. (c) Velocity vectors and plug regions for Newtonian fluid (left), mide range yield number (midle), and high yield number (right) at $\boldsymbol{Ra} = 10^6$, $\boldsymbol{Nr} = 1$, and $\boldsymbol{Le} = 1$.

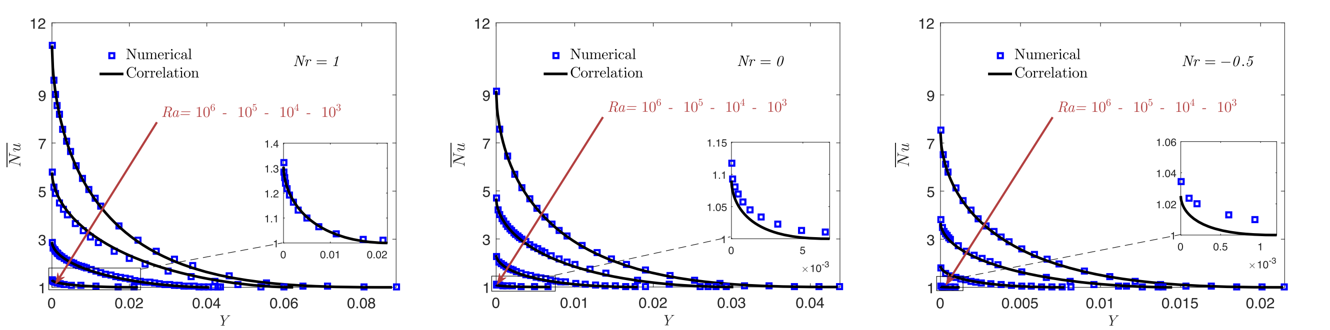

Fig. 6. Variations of mean Nusselt number $\overline{\boldsymbol{Nu}}$ with yield number, $\boldsymbol{Y}$, for cooperative buoyancy convection (left), thermal buoyancy convection (midle), and opposing solutal buoyancy force (right) at $\boldsymbol{Ra} = 10^3 - 10^6$ and $\boldsymbol{Le} = 1$.

The numerical solution results are then used to calculate the parameters and coefficients involved in the equation.

First, a correlation for the mean Nusselt number of Newtonian fluids $\overline{Nu}_N$ is given as follows:

$$\overline{Nu}_N = a_n Ra^{b_n} + c_n \tag{19}$$

Where:

$$\begin{aligned} a_n &= 0.2841\exp(0.1573Nr) - 0.08509\exp(-1.449Nr) \\ b_n &= 0.01755\exp(-2.359Nr) + 0.2618\exp(-0.005785Nr) \\ c_n &= -0.3439\exp(0.5629Nr) + 0.06353\exp(-4.098Nr) \end{aligned} \tag{20}$$

This new correlation has improved the results of the previous correlation, especially in low Rayleigh numbers (Table 2).

The correlation of maximum yield number can be defined as:

$$Y_{max} = a_Y Ra^{b_Y} + c_Y \tag{21}$$

Where:

$$\begin{aligned} a_Y &= 0.05529\exp(-2.29Nr) + 0.03987\exp(0.3725Nr) \\ b_Y &= 0.04826\exp(0.4097Nr) - 0.01067\exp(-1.849Nr) \\ c_Y &= -0.02921\exp(-3.032Nr) - 0.08729\exp(-0.08665Nr) \end{aligned} \tag{22}$$

Y_{max}represents the maximum amount of stress causing the Nusselt number to converge to one, indicating conductive heat transfer in the cavity.

Table 2
Comparison of the measured $\overline{Nu}_N$ with the correlations (present study and Beghein study [10]).

Ra	$\overline{Nu}_N$														
	Nr														
	1					0					− 0.5				
	PresentStudy		BegheinStudy		Num.Data	PresentStudy		BegheinStudy		NumData	PresentStudy		BegheinStudy		NumData
	Value	Error	Value	Error		Value	Error	Value	Error		Value	Error	Value	Error	
10^3	1.306	1.14%	1.712	29.65%	1.321	1.090	2.39%	1.420	27.16%	1.117	1.025	0.86%	1.178	13.92%	1.034
10^4	2.886	1.12%	3.189	11.75%	2.854	2.327	2.39%	2.645	16.36%	2.273	1.886	5.07%	2.193	22.2%	1.795
10^5	5.774	0.36%	5.938	2.48%	5.795	4.681	0.75%	4.925	4.41%	4.717	3.683	3.45%	4.084	7.06%	3.815
10^6	11.053	0.04%	11.058	0.09%	11.048	9.159	0.07%	9.171	0.19%	9.153	7.435	1.43%	7.6	0.82%	7.543

Finally, the coefficients a and b are calculated as follows:

$$\begin{aligned} a &= 0.56 \\ b &= a'.exp(b'.Ra) + c'.exp(d'.Ra) \end{aligned} \tag{23}$$

The coefficients used in the above relation are calculated as follows:

$$\begin{aligned} a' &= 0.1177\exp(-1.036Nr) + 0.3043\exp(0.07423Nr) \\ b' &= -0.0001837\exp(0.3779Nr) + 0.00002618\exp(-2.236Nr) \\ c' &= 2.223\exp(-0.2657Nr) - 0.3826\exp(-1.471Nr) \\ d' &= \left(\left(4.291 * 10^{-9}\right).exp(-5.667Nr) + \left(3.153 * 10^{-7}\right).\exp(0.4724Nr)\right) \end{aligned} \tag{24}$$

The results of the numerical solution and correlation are depicted in Fig. 6. There is a high degree of agreement between the outcomes. Table 3 shows the relative difference between the correlation and the numerical findings.

4.2. Effects of Lewis number

This section examines the combined effects of yield stress (Y), buoyancy ratio number (Nr), and Lewis number (Le) on the fluid flow and both the thermal and concentration fields for Casson fluid. Fig. 7 shows the effects of Lewis number and buoyancy ratio on velocity, v, and concentration, C. One can observe that the fluid velocity profiles have quite the opposite behavior for $Nr = -0.5$compared with $Nr = 1$. In the assisting flow, increasing the Lewis number decreases the positive effect of Nr and thus decreases the flow strength. Still, in the opposing flow, the Lewis number reduces the negative effect of Nr, and the flow strength increases. However, with increasing Lewis number, the concentration distribution becomes nonuniform for both aiding and opposing solutal buoyancy force, representing the direct relationship between mass distribution and Lewis number in both cases.

The combined effects of Lewis and buoyancy ratio numbers on stream function and morphology of yielded/unyielded regions are shown in Fig. 8. Results show that as the Lewis number increases, the effects of the buoyancy ratio parameter on flow characteristics decrease for both aiding and opposing solutal buoyancy force. Hence, for $Nr = -0.5$, the flow becomes stronger, and the unyielded regions decrease with increasing the Lewis number, while an opposite trend can be seen for assisting flow ($Nr = 1$). This is due to the high intensity of mass distribution at high Lewis numbers, as seen in concentration contours. However, it is worth noting that the overall shape of the flow pattern and the unyielded areas are determined by the buoyancy ratio (see the red dot lines).

Fig. 9 depicts the combined influence of yield number (Y), buoyancy ratio (Nr), and the Lewis number (Le) on the mean Nusselt number. Similar results for the Sherwood number are shown in Fig. 10. It is observed that the mean Nusselt number for assisting flow ($Nr = 1$) decreases with increasing Le, while an opposite trend could be observed for $Nr = -0.5$. This must occur because, as previously described, increasing Le reduces the effect of the solutal buoyancy force. However, in the case of $Nr = 0$, because concentration does not affect buoyancy force, the amount of heat transfer is independent of the Lewis number. On the other hand, the results show that for high Lewis numbers ($Le = 5$, 10), there is an insignificant change in $\overline{Nu}$.

As mentioned above, increasing the Lewis number enhances mass transfer in the cavity. Consequently, the average Sherwood number increases significantly when the Lewis number rises. According to the findings, when the Lewis number rises, the rate of mass transmission can increase by up to three times that of heat transfer. However, as previously indicated, increasing the Lewis number decreases the effect of the buoyancy ratio on heat transfer. As a result, for $Nr > 0$, there is a rise in the gap between the Nusselt and Sherwood numbers. For $Nr < 0$, however, the relative difference between Nusselt and Sherwood numbers decreases.

From these figures, it is apparent that heat and mass transfer decrease as the yield number increases. However, the effect of yield stress is more significant for the opposing flow ($Nr = -0.5$). Results show an abrupt change in Sherwood number at high yield numbers due to the dominance of viscous force (especially for higher Lewis numbers).

4.2.1. Correlation for the Nusselt number

Based on the explanations in the previous section (4.1.1), a correlation for the mean Nusselt number of yield stress Casson fluid)$\overline{Nu}$(corresponding to different values of Lewis number (Le), buoyancy ratio number (Nr), and yield number (Y) can be proposed in a general form as below:

$$\overline{Nu} = 1 + \left(\overline{Nu}_N - 1\right)\left[1 - \left(\frac{Y}{Y_{max}}\right)^{a}\right]^{b} \tag{25}$$

The mean Nusselt number of Newtonian fluids $\overline{Nu}_N$, maximum yield number Y_{max}, and the coefficients a and b are summarized in Table 4.

The results of the numerical solution and correlation are depicted in Fig. 8. There is a high degree of agreement between the outcomes. Table 5 shows the relative difference between the correlation and numerical values.

4.2.2. Correlation for the Sherwood number

The correlation of the Sherwood number is more complicated than the Nusselt number. This is (as mentioned earlier) due to the abrupt change in the Sherwood diagram. Similar to what was done for the Nusselt number (Section 4.1.1), the correlation for the mean Sherwood number ($\overline{Sh}$) corresponding to different values of Lewis number (Le),

Table 3
Relative difference between the correlation and numerical results.

Ra	Error(%)		
	Nr		
	1	0	− 0.5
10^6	0.79	0.86	1.31
10^5	2.08	2.81	2.44
10^4	0.66	1.88	1.67
10^3	0.47	2.45	1.23

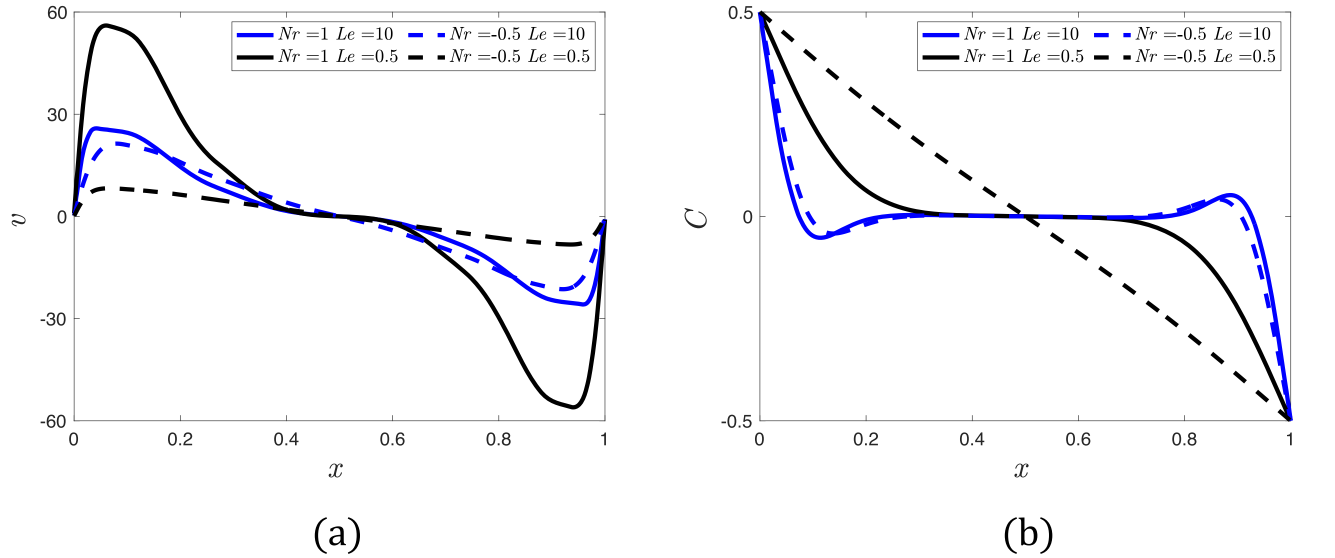

Fig. 7. Effects of Lewis number on velocity and concentration distribution: (a) Variations of non-dimensional velocity along the horizontal mid-plane. (b) Variations of non-dimensional concentration along the horizontal mid-plane. ($\boldsymbol{Ra} = 10^5, \boldsymbol{Y} = 0.005$).

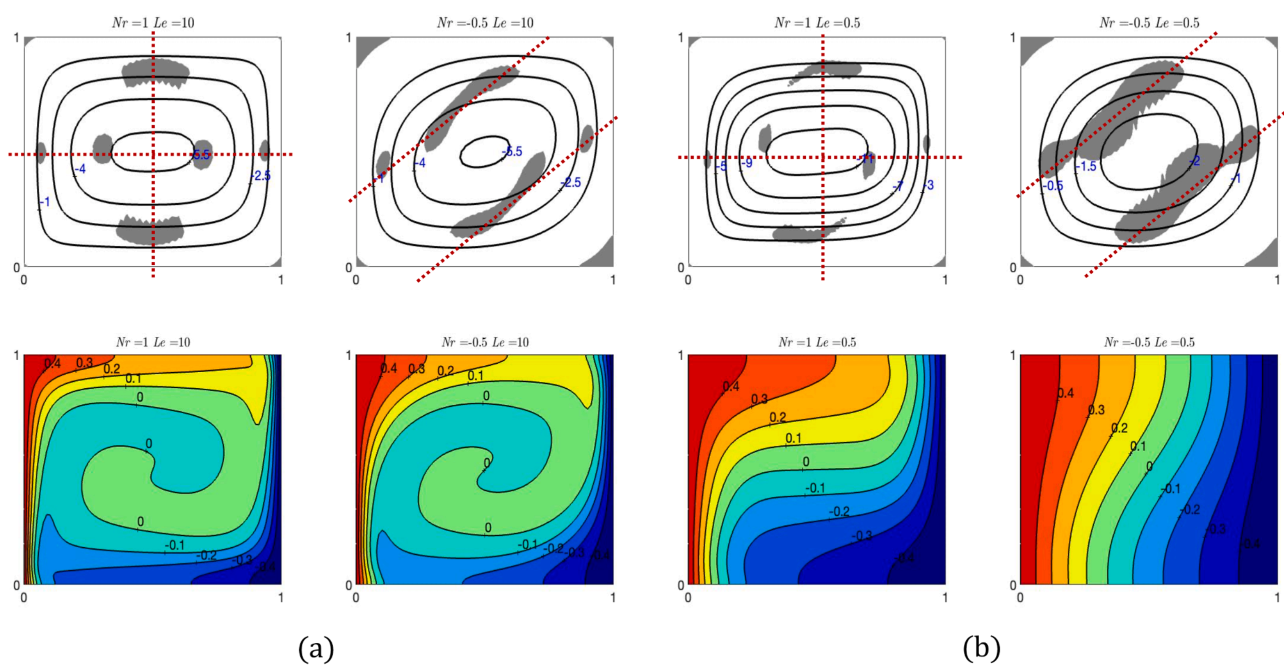

Fig. 8. Effects of Lewis number on stream functions and concentration contours: (a) Contours of non-dimensional stream functions and concentration at Le=10 for cooperative buoyancy convection (left) and opposing solutal buoyancy force (right) (b) Contours of non-dimensional stream functions and concentration at Le=0.5 for cooperative buoyancy convection (left) and opposing solutal buoyancy force (right). The red dot lines indicate that the overall shape of the flow pattern and unyielded areas in the cavity is determined by the buoyancy ratio. ($\boldsymbol{Ra} = 10^5, \boldsymbol{Y} = 0.005$).

buoyancy ratio number (*Nr*), and yield number *(Y)* can be proposed as below:

$$\overline{Sh} = \overline{Sh}_m + (\overline{Sh}_N - \overline{Sh}_m)\left[1 - \left(\frac{Y}{Y_{max}}\right)^a\right]^b \tag{26}$$

The mean Sherwood number of Newtonian fluids $\overline{Sh}_N$, minimum Sherwood number $\overline{Sh}_m$, and the coefficients *a* and *b* are summarized in Table 6.

Fig. 10 shows the results of numerical solution and correlation. There is a good agreement between the results (Table 7).

5. Conclusions

The analysis of double-diffusion natural convection of Casson fluid was extended in this study to the flow within the enclosure. The governing equations and the numerical solution model were derived based on the geometry of the problem and its boundary conditions. Additionally, the original Casson fluid stress model was used without simplification in this study. Consequently, the findings were acquired and evaluated based on the yield stress and its influence on heat and mass transmission, as well as the formation and development of unyielding zones. Various representative numerical results were presented for a variety of control parameters, including Rayleigh number, yield

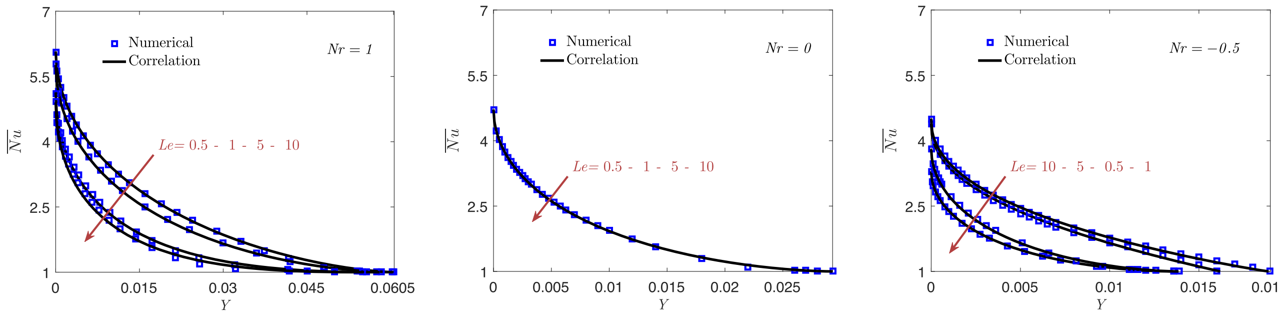

Fig. 9. Variations of mean Nusselt number $\overline{Nu}$ with yield number, Y, for cooperative buoyancy convection (left), thermal buoyancy convection (midle), and opposing solutal buoyancy force (right) at $Le = -0.5$, 0, 5, 10 and $Ra = 10^5$.

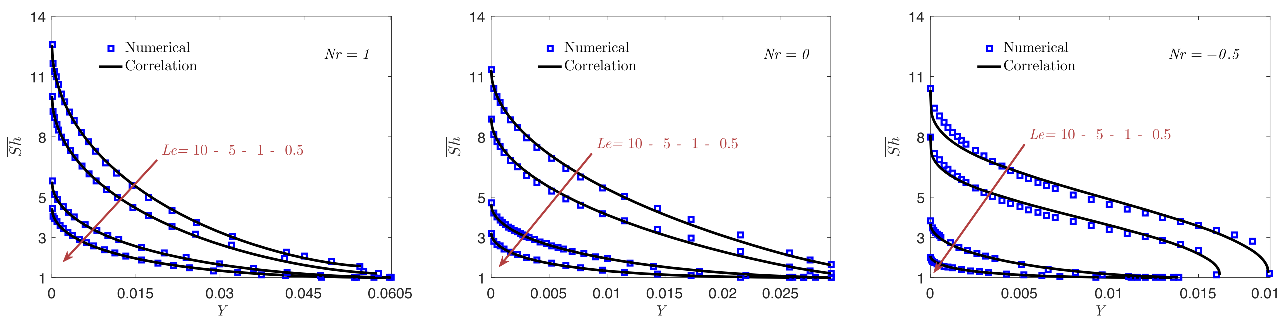

Fig. 10. Variations of mean Sherwood number $\overline{Sh}$ with yield number, Y, for cooperative buoyancy convection (left), thermal buoyancy convection (midle), and opposing solutal buoyancy force (right) at$Le = -0.5$, 0, 5, 10 and $Ra = 10^5$.

Table 4
Scaling laws for Newtonian Nusselt number $\overline{Nu}_N$, maximum yield number Y_{max}, and the coefficient$a$ and b.

Nr	$\overline{Nu}_N$	Y_{max}	b		a	
1	$3.24Le^{-0.1335} + 2.522$	$-0.0005923Le^{0.9898} + 0.06092$	$2.292.exp(0.005028.Le) - 1.004.exp(-0.4611.Le)$		0.52	
0	4.717	0.0293	1.64		0.52	
−0.5	$-0.9008Le^{-0.6486} + 4.71$	$0.0006771Le^{0.927} + 0.01318$	$Le \leq 1$	$Le > 1$	$Le \leq 1$	$Le > 1$
			$1.75.exp(-0.0597.Le)$	$0.935.exp(0.0135.Le)$	0.52	0.44

Table 5
Relative difference between the correlation and numerical results of $\overline{Nu}$ (Effects of Lewis number).

Le	$Error$ (%)		
	Nr		
	1	0	−0.5
0.5	0.95	0.61	0.44
1	0.85	0.61	1.28
5	1.57	0.61	1.46
10	2.62	0.61	1.15

number, buoyancy ratio, and Lewis number. The research results are concluded as below.

Effects of Rayleigh number: It is observed that increased buoyancy owing to a rise in Rayleigh number lessens the influence of yield stress on heat and mass transmission. On the other hand, increasing the convective force causes the flow to be more closely confined to the walls due to stronger circulation. Thus, the shear rate in the central areas of the enclosure decreases, resulting in the growth of unyielded areas. Because of this, with an increasing Rayleigh number, the areas closest to the wall will experience the most significant changes in temperature and

Table 7
Relative difference between the correlation and numerical results of $\overline{Sh}$ (Effects of Lewis number).

Le	$Error$ (%)		
	Nr		
	1	0	−0.5
0.5	1	0.81	1.33
1	1.31	1.1	2.8
5	1.03	2.54	4.11
10	1.14	2.14	4.39

Table 6
Scaling laws for Newtonian Sherwood number $\overline{Sh}_N$, minimum Sherwood number $\overline{Sh}_m$, and the coefficients a and b.

Nr	$\overline{Sh}_N$	$\overline{Sh}_m$	b	a	
1	$7.574Le^{0.2776} - 1.801$	$0.02424Le^{1.382} + 0.99$	$0.996.exp(-1.575.Le) + 1.5.exp(-0.0041.Le)$	0.52	
0	$9.497Le^{0.2314} - 4.858$	$0.01829Le^{1.541} + 0.9941$	$2.71.exp(-1.87.Le) + 1.191.exp(-0.00704.Le)$	0.52	
−0.5	$16.84Le^{0.1447} - 13.16$	$0.04844Le^{0.7282} + 0.971$	$3.12.exp(-1.037.Le) + 0.4408.exp(0.007446.Le)$	$Le \leq 1$	$Le > 1$
				0.52	0.25

mass distribution, while in the unyielded areas of the center, such changes will be negligible.

Effects of buoyancy ratio: Compared to Newtonian fluids, the beneficial effect of the positive buoyancy ratio is less pronounced in Casson fluids because of stronger viscous force. On the other hand, the adverse impact of the opposing solutal buoyancy force on heat and mass transport grows. Plug regions are visible in all cases, but at negative buoyancy ratios, these zones occupy more space in the enclosure. In other words, a positive buoyancy force act as a deterrent to the growth of plug regions, while an opposing buoyancy force stimulates their growth.

Effects of the yield number: The results indicated that the yield number plays a crucial role in the heat and mass transfer of the Casson fluid in the enclosure. By increasing the yield stress, the viscosity increases, and the strength of the buoyancy force is reduced. Thus, a more uniform temperature and concentration distribution can be observed in the cavity. As a result, unyielded regions grow with increasing Y. The combined effect of increasing the yield number and decreasing the buoyancy ratio causes the unyielded areas to invade the whole cavity, indicating conduction-driven transport.

Effects of the Lewis number: It is observed that, in general, increasing the Lewis number reduces the effect of the buoyancy ratio. Therefore, for $Nr < 0$, the unyielded regions decrease as the Lewis number increases. However, yield stress and Lewis number have similar effects on plug regions in positive buoyancy ratios. As a result, in this case, unyielded areas increase with increasing Lewis number. According to the results, the maximum yield stress is more a function of temperature and flow than concentration. Therefore, at high Lewis numbers and negative buoyancy ratios, an abrupt change in the Sherwood number is observed in the maximum yield stress zone.

CRediT authorship contribution statement

M.S. Aghighi: Supervision, Conceptualization, Methodology, Software, Writing – original draft. **A. Ammar:** Supervision, Conceptualization, Writing – review & editing. **H. Masoumi:** Data curation, Visualization, Investigation, Validation.

Declaration of Competing Interest

The authors declare that they have no known competing financial interests or personal relationships that could have appeared to influence the work reported in this paper.

Data Availability

The data that has been used is confidential.

References

[1] Turner JS. Double-diffusive phenomena. Annu Rev Fluid Mech 1974;6(1):37–54. https://doi.org/10.1146/annurev.fl.06.010174.000345.
[2] Huppert HE, Moore DR. Nonlinear double-diffusive convection. J Fluid Mech 1976;78(4):821–54.
[3] Linden PF, Shirtcliffe TGL. The diffusive interface in double-diffusive convection. J Fluid Mech 1978;87(3):417–32. https://doi.org/10.1017/S002211207800169X.
[4] Griffiths RW. Layered double-diffusive convection in porous media. J Fluid Mech 1979;5(1978):221–48.
[5] da Costa LN, Knobloch E, Weiss NO. Oscillations in double-diffusive convection. J Fluid Mech 1981;109:25–43. https://doi.org/10.1017/S0022112081000918.
[6] Knobloch E, Proctor MRE. Nonlinear periodic convection in double-diffusive systems. J Fluid Mech 1981;108:291–316. https://doi.org/10.1017/S0022112081002139.
[7] Huppert H, Turner S. Double-diffusive convection. J Fluid Mech 1981;106:299–329.
[8] Han H, Kuehn TH. Double diffusive natural convection in a vertical rectangular enclosure-I. Experimental study. Int J Heat Mass Transf 1991;34(2):449–59. https://doi.org/10.1016/0017-9310(91)90264-F.
[9] Han H, Kuehn TH. Double diffusive natural convection in a vertical rectangular enclosure-II. Numerical study. Int J Heat Mass Transf 1991;34(2):461–71. https://doi.org/10.1016/0017-9310(91)90265-G.
[10] Béghein C, Haghighat F, Allard F. Numerical study of double-diffusive natural convection in a square cavity. Int J Heat Mass Transf 1992;35(4):833–46. https://doi.org/10.1016/0017-9310(92)90251-M.
[11] Mamou M, Vasseur P, Bilgen E. Analytical and numerical study of double diffusive convection in a vertical enclosure. Heat and Mass Transfer 1996;32(1):115–25. https://doi.org/10.1007/S002310050100.
[12] Xin S, le Quéré P, Tuckerman LS. Bifurcation analysis of double-diffusive convection with opposing horizontal thermal and solutal gradients. Phys Fluids 1998;10(4):850. https://doi.org/10.1063/1.869608.
[13] Ghorayeb K, Mojtabi A. Double diffusive convection in a vertical rectangular cavity. Phys Fluids 1997;9(8):2339–48. https://doi.org/10.1063/1.869354.
[14] van der Eyden JT, van der Meer TH, Hanjalić K, Biezen E, Bruining J. Double-diffusive natural convection in trapezoidal enclosures. Int J Heat Mass Transf 1998;41(13):1885–98. https://doi.org/10.1016/S0017-9310(97)00353-0.
[15] Mamou M, Vasseur P, Bilgen E. Multiple solutions for double-diffusive convection in a vertical porous enclosure. Int J Heat Mass Transf 1995;38(10):1787–98. https://doi.org/10.1016/0017-9310(94)00301-B.
[16] Karimi-Fard M, Charrier-Mojtabi MC, Vafai K. Non-Darcian Effects on Double-Diffusive Convection Within a Porous Medium. Numer Heat Transfer, Part A Jun. 1997;31(8):837–52. https://doi.org/10.1080/10407789708914067.
[17] Nithiarasu P, Seetharamu KN, Sundararajan T. Double-Diffusive Natural Convection in an Enclosure Filled With Fluid-Saturated Porous Medium: a Generalized Non-Darcy Approach. Numer Heat Transf, Part A 1996;30(4):413–26. https://doi.org/10.1080/10407789608913848.
[18] Bennacer R, Tobbal A, Beji H, Vasseur P. Double diffusive convection in a vertical enclosure filled with anisotropic porous media. Int J Therm Sci 2001;40(1):30–41. https://doi.org/10.1016/S1290-0729(00)01185-6.
[19] Nield DA, Kuznetsov Av. The onset of double-diffusive convection in a nanofluid layer. Int J Heat Fluid Flow 2011;32(4):771–6. https://doi.org/10.1016/j.ijheatfluidflow.2011.03.010.
[20] Kuznetsov Av, Nield DA. Double-diffusive natural convective boundary-layer flow of a nanofluid past a vertical plate. Int J Therm Sci 2011;50(5):712–7. https://doi.org/10.1016/j.ijthermalsci.2011.01.003.
[21] Sheikhzadeh GA, Dastmalchi M, Khorasanizadeh H. Effects of walls temperature variation on double diffusive natural convection of Al2O3-water nanofluid in an enclosure. Heat Mass Transfer 2013;49(12):1689–700. https://doi.org/10.1007/s00231-013-1209-9.
[22] Hussain S, Öztop HF, Jamal M, Hamdeh NA. Double diffusive nanofluid flow in a duct with cavity heated from below. Int J Mech Sci 2017;131–132:535–45. https://doi.org/10.1016/j.ijmecsci.2017.07.057.
[23] He B, Lu S, Gao D, Chen W, Li X. Lattice Boltzmann simulation of double diffusive natural convection of nanofluids in an enclosure with heat conducting partitions and sinusoidal boundary conditions. Int J Mech Sci 2019:161–2. https://doi.org/10.1016/j.ijmecsci.2019.07.002.
[24] Sharma A, Tripathi D, Sharma RK, Tiwari AK. Analysis of double diffusive convection in electroosmosis regulated peristaltic transport of nanofluids. Physica A 2019;535:122148. https://doi.org/10.1016/j.physa.2019.122148.
[25] Raizah Z, Aly AM. Double-diffusive convection of a rotating circular cylinder in a porous cavity suspended by nano-encapsulated phase change materials. Case Stud Therm Eng 2021;24(November 2020):100864. https://doi.org/10.1016/j.csite.2021.100864.
[26] Mondal P, Mahapatra TR. MHD double-diffusive mixed convection and entropy generation of nanofluid in a trapezoidal cavity. Int J Mech Sci 2021;208:106665. https://doi.org/10.1016/J.IJMECSCI.2021.106665.
[27] Sunil ASharma, Kumar Bharti P, Shandil RG. Linear stability of double-diffusive convection in a micropolar ferromagnetic fluid saturating a porous medium. Int J Mech Sci 2007;49(9):1047–59. https://doi.org/10.1016/j.ijmecsci.2007.01.002.
[28] Teamah MA. Numerical simulation of double diffusive natural convection in rectangular enclosure in the presences of magnetic field and heat source. Int J Therm Sci 2008;47(3):237–48. https://doi.org/10.1016/j.ijthermalsci.2007.02.003.
[29] Teamah MA, Elsafty AF, Elfeky MZ, El-Gazzar EZ. Numerical simulation of double-diffusive natural convective flow in an inclined rectangular enclosure in the presence of magnetic field and heat source, part A: effect of Rayleigh number and inclination angle. Alexandria Eng J 2011;50(4):269–82. https://doi.org/10.1016/j.aej.2010.05.001.
[30] Prakash J, Sharma A, Tripathi D. Convective heat transfer and double diffusive convection in ionic nanofluids flow driven by peristalsis and electromagnetohydrodynamics. Pramana - J Phys 2020;94(1). https://doi.org/10.1007/s12043-019-1873-5.
[31] Vijaybabu TR. Influence of porous circular cylinder on MHD double-diffusive natural convection and entropy generation. Int J Mech Sci 2021;206:106625. https://doi.org/10.1016/j.ijmecsci.2021.106625.
[32] Hu JT, Mei SJ, Liu D, Zhao FY, Wang HQ. Hydromagnetic double diffusive moisture convection from an inclined enclosure inserted with multiple heat-generating electronic modules. Int J Therm Sci 2021;159:106554. https://doi.org/10.1016/J.IJTHERMALSCI.2020.106554.
[33] Kushawaha D, Yadav S, Singh DK. Magnetic field effect on double-diffusion with magnetic and non-magnetic nanofluids. Int J Mech Sci 2021;191:106085. https://doi.org/10.1016/J.IJMECSCI.2020.106085.
[34] Vijaybabu TR. Impression of porous body and magnetic field on the double-diffusive mixed convection traits. Int J Mech Sci 2022;215:106955. https://doi.org/10.1016/J.IJMECSCI.2021.106955.
[35] Chen S, Du R. Entropy generation of turbulent double-diffusive natural convection in a rectangle cavity. Energy 2011;36(3):1721–34. https://doi.org/10.1016/j.energy.2010.12.056.

[36] Oueslati F, Ben-Beya B, Lili T. Double-diffusive natural convection and entropy generation in an enclosure of aspect ratio 4 with partial vertical heating and salting sources. Alexandria Eng J 2013;52(4):605–25. https://doi.org/10.1016/j.aej.2013.09.006.
[37] Siavashi M, Bordbar V, Rahnama P. Heat transfer and entropy generation study of non-Darcy double-diffusive natural convection in inclined porous enclosures with different source configurations. Appl Therm Eng 2017;110:1462–75. https://doi.org/10.1016/j.applthermaleng.2016.09.060.
[38] Nithyadevi N, Yang RJ. Double diffusive natural convection in a partially heated enclosure with Soret and Dufour effects. Int J Heat Fluid Flow 2009;30(5):902–10. https://doi.org/10.1016/j.ijheatfluidflow.2009.04.001.
[39] Wang J, Yang M, Zhang Y. Onset of double-diffusive convection in horizontal cavity with Soret and Dufour effects. Int J Heat Mass Transf 2014;78:1023–31. https://doi.org/10.1016/j.ijheatmasstransfer.2014.07.064.
[40] Wang J, Yang M, He YL, Zhang Y. Oscillatory double-diffusive convection in a horizontal cavity with Soret and Dufour effects. Int J Therm Sci 2016;106:57–69. https://doi.org/10.1016/j.ijthermalsci.2016.03.012.
[41] Ren Q, Chan CL. Numerical study of double-diffusive convection in a vertical cavity with Soret and Dufour effects by lattice Boltzmann method on GPU. Int J Heat Mass Transf 2016;93:538–53. https://doi.org/10.1016/j.ijheatmasstransfer.2015.10.031.
[42] Muthtamilselvan M, Periyadurai K, Doh DH. Impact of nonuniform heated plate on double-diffusive natural convection of micropolar fluid in a square cavity with Soret and Dufour effects. Adv Powder Technol 2018;29(1):66–77. https://doi.org/10.1016/j.apt.2017.10.012.
[43] Al-Mudhaf AF, Rashad AM, Ahmed SE, Chamkha AJ, EL-Kabeir SMM. Soret and Dufour effects on unsteady double diffusive natural convection in porous trapezoidal enclosures. Int J Mech Sci May 2018;140:172–8. https://doi.org/10.1016/j.ijmecsci.2018.02.049.
[44] Makayssi T, Lamsaadi M, Naïmi M, Hasnaoui M, Raji A, Bahlaoui A. Natural double-diffusive convection in a shallow horizontal rectangular cavity uniformly heated and salted from the side and filled with non-Newtonian power-law fluids: the cooperating case. Energy Convers Manage 2008;49(8):2016–25. https://doi.org/10.1016/j.enconman.2008.02.008.
[45] Kefayati GHR. Double-diffusive natural convection and entropy generation of Bingham fluid in an inclined cavity. Int J Heat Mass Transf 2018;116:762–812. https://doi.org/10.1016/j.ijheatmasstransfer.2017.09.065.
[46] Kumar SBN, Shivakumara IS, Shankar BM. Linear and weakly nonlinear double-diffusive magnetoconvection in a non-newtonian fluid layer. Microgravity Sci Technol 2020;32(4):629–46. https://doi.org/10.1007/s12217-020-09781-4.
[47] Tizakast Y, Kaddiri M, Lamsaadi M. Double-diffusive mixed convection in rectangular cavities filled with non-Newtonian fluids. Int J Mech Sci 2021;208:106667. https://doi.org/10.1016/J.IJMECSCI.2021.106667.
[48] Bihiche K, Lamsaadi M, Hasnaoui M. Multiple steady state solutions for double-diffusive convection in a shallow horizontal rectangular cavity uniformly heated and salted from the side and filled with non-Newtonian power-law fluids. J Nonnewton Fluid Mech 2020;283:104349. https://doi.org/10.1016/J.JNNFM.2020.104349.
[49] Yadav D, et al. Double diffusive convective motion in a reactive porous medium layer saturated by a non-Newtonian Kuvshiniski fluid. Phys Fluids 2022;34(2):024104. https://doi.org/10.1063/5.0083378.
[50] Bingham E. The behavior of plastic materials. Bull. US Bureau Standard 1916;13:309–53.
[51] Herschel WH, Bulkley R. Measurement of consistency as applied to rubber-benzene solutions. Am Soc Test Proc 1926;26(2).
[52] Casson N. Rheology of Disperse Systems. Oxford: Pergamon Press; 1959.
[53] Turan O, Chakraborty N, Poole RJ. Laminar natural convection of Bingham fluids in a square enclosure with differentially heated side walls. J Nonnewton Fluid Mech 2010;165(15–16):901–13. https://doi.org/10.1016/j.jnnfm.2010.04.013.
[54] Karimfazli I, Frigaard IA. Natural convection flows of a Bingham fluid in a long vertical channel. J Nonnewton Fluid Mech 2013;201:39–55. https://doi.org/10.1016/j.jnnfm.2013.07.003.
[55] Yigit S, Chen S, Quinn P, Chakraborty N. Numerical investigation of laminar Rayleigh-Bénard convection of Bingham fluids in square cross-sectioned cylindrical enclosures. Int J Therm Sci 2016;110:356–68. https://doi.org/10.1016/j.ijthermalsci.2016.07.013.
[56] Rafiei B, Masoumi H, Aghighi MS, Ammar A. Effects of complex boundary conditions on natural convection of a viscoplastic fluid. Int J Numer Methods Heat Fluid Flow 2019;29(8). https://doi.org/10.1108/HFF-09-2018-0507.
[57] Masoumi H, Aghighi MS, Ammar A, Nourbakhsh A. Laminar natural convection of yield stress fluids in annular spaces between concentric cylinders. Int J Heat Mass Transf 2019;138:1188–98. https://doi.org/10.1016/j.ijheatmasstransfer.2019.04.092.
[58] Aghighi MS, Ammar A, Masoumi H, Lanjabi A. Rayleigh–Bénard convection of a viscoplastic liquid in a trapezoidal enclosure. Int J Mech Sci 2020;180:105630. https://doi.org/10.1016/j.ijmecsci.2020.105630.
[59] Hassan MA, Pathak M, Khan MK. Rayleigh-Benard convection in Herschel-Bulkley fluid. J Nonnewton Fluid Mech 2015;226:32–45. https://doi.org/10.1016/j.jnnfm.2015.10.003.
[60] Aghighi MS, Ammar A. Aspect ratio effects in Rayleigh-Bénard convection of Herschel-Bulkley fluids. Eng Comput 2017;34(5). https://doi.org/10.1108/EC-06-2016-0227.
[61] Aghighi MS, Ammar A, Metivier C, Gharagozlu M. Rayleigh-Bénard convection of Casson fluids. Int J Therm Sci 2018;127:79–90. https://doi.org/10.1016/j.ijthermalsci.2018.01.016.
[62] Aghighi MS, Metivier C, Masoumi H. Natural convection of Casson fluid in a square enclosure. Multidiscip Model Mater Struct 2020;16(5):1245–59. https://doi.org/10.1108/MMMS-11-2019-0192.
[63] Scott Blair GW. The success of Casson's equation. Rheol Acta Sep. 1966;5(3):184–7. https://doi.org/10.1007/BF01982424.
[64] Mitsoulis E. Flows of viscoplastic materials: models and computations. Rheol Rev 2007;2007:135–78. https://doi.org/10.1016/S0045-7949(96)00167-8.
[65] Mohan CG, Satheesh A. The numerical simulation of double-diffusive mixed convection flow in a lid-driven porous cavity with magnetohydrodynamic effect. Arab J Sci Eng 2016;41(5):1867–82. https://doi.org/10.1007/s13369-015-1998-x.
[66] Ahmed SE, Mansour MA, Mahdy A, Mohamed SS. Entropy generation due to double diffusive convective flow of Casson fluids over nonlinearity stretching sheets with slip conditions. Eng Sci Technol Int J 2017;20(6):1553–62. https://doi.org/10.1016/j.jestch.2017.10.002.
[67] Gireesha BJ, Archana M, Prasannakumara BC, Reddy Gorla RS, Makinde OD. MHD three dimensional double diffusive flow of Casson nanofluid with buoyancy forces and nonlinear thermal radiation over a stretching surface. Int J Numer Methods Heat Fluid Flow 2017;27(12):2858–78. https://doi.org/10.1108/HFF-01-2017-0022.
[68] Das M, Mahanta G, Shaw S, Parida SB. Unsteady MHD chemically reactive double-diffusive Casson fluid past a flat plate in porous medium with heat and mass transfer. Heat Transfer Asian Res 2019;48(5):1761–77. https://doi.org/10.1002/htj.21456.
[69] Oyelakin IS, Lalramneihmawii PC, Mondal S, Sibanda P. Analysis of double-diffusion convection on three-dimensional MHD stagnation point flow of a tangent hyperbolic Casson nanofluid. Int J Ambient Energy 2020:1–23. https://doi.org/10.1080/01430750.2020.1722964. vol. 0, no. 0.
[70] Pal D, Roy N. Lie group transformation on MHD double-diffusion convection of a casson nanofluid over a vertical stretching/shrinking surface with thermal radiation and chemical reaction. Int J Appl Comput Math 2017;4(1):1–23. https://doi.org/10.1007/S40819-017-0449-7.
[71] Prasad DVK, Chaitanya GSK, Raju RS. Double diffusive effects on mixed convection Casson fluid flow past a wavy inclined plate in presence of Darcian porous medium. Result Eng 2019;3:100019. https://doi.org/10.1016/j.rineng.2019.100019.
[72] Mahanta G, Das M, Shaw S, Mahala BK. Mhd double-diffusive thermosolutal marangoni convection non-newtonian casson fluid flow over a permeable stretchable sheet. Heat Transfer 2020;49(4):1788–807. https://doi.org/10.1002/htj.21691.
[73] Kumar A, Tripathi R, Singh R, Sheremet MA. Entropy generation on double diffusive MHD Casson nanofluid flow with convective heat transfer and activation energy. Indian J Phys 2021;95(7):1423–36. https://doi.org/10.1007/s12648-020-01800-9.
[74] Gupta U, Sharma J, Devi M. Double-diffusive instability of Casson nanofluids with numerical investigations for blood-based fluid. Eur Phys J Spec Top 2021;230(5):1435–45. https://doi.org/10.1140/EPJS/S11734-021-00053-9.
[75] Papanastasiou TC. Flows of materials with yield. J Rheol (N Y N Y) 1987;31(5):385–404. https://doi.org/10.1122/1.549926.
[76] Djebali R, Mebarek-Oudina F, Rajashekhar C. Similarity solution analysis of dynamic and thermal boundary layers: further formulation along a vertical flat plate. Phys Scr 2021;96(8):085206. https://doi.org/10.1088/1402-4896/ABFE31.
[77] Asogwa KK, Mebarek-Oudina F, Animasaun IL. Comparative investigation of water-based Al2O3 nanoparticles through water-based CuO nanoparticles over an exponentially accelerated radiative riga plate surface via heat transport. Arab J Sci Eng 2022:1–18. https://doi.org/10.1007/S13369-021-06355-3.
[78] Warke AS, Ramesh K, Mebarek-Oudina F, Abidi A. Numerical investigation of the stagnation point flow of radiative magnetomicropolar liquid past a heated porous stretching sheet. J Therm Anal Calorim 2021;147(12):6901–12. https://doi.org/10.1007/S10973-021-10976-Z.
[79] Roy S, Basak T. Finite element analysis of natural convection flows in a square cavity with non-uniformly heated wall(s). Int J Eng Sci 2005;43(8–9):668–80. https://doi.org/10.1016/j.ijengsci.2005.01.002.
[80] Aghighi MS, Ammar A, Metivier C, Normandin M, Chinesta F. Non-incremental transient solution of the Rayleigh-Bénard convection model by using the PGD. J Nonnewton Fluid Mech 2013;200. https://doi.org/10.1016/j.jnnfm.2012.11.007.
[81] Al-Weheibi SM, Rahman MM, Alam MS, Vajravelu K. Numerical simulation of natural convection heat transfer in a trapezoidal enclosure filled with nanoparticles. Int J Mech Sci 2017;131–132:599–612. https://doi.org/10.1016/j.ijmecsci.2017.08.005.